SCIEPublish

Article

A Shear Stress Model for Magnetorheological Fluid with High Volume Fraction

Yanhui Tao [1,2], Changhong Cao [2], Yong Huang [2], Ping Xiao [2], Liang Ma [2,*] and Cong Sun [3,*]

[1] Xinjiang Coal Mine Electromechanical Engineering Technology Research Center, Xinjiang Institute of Engineering, Urumqi 830023, China; taoyanhui1102@sina.com (Y.T.)

[2] School of Mechanical and Electrical Engineering, Xinjiang Institute of Engineering, Urumqi 830023, China; caoch24@mails.jlu.edu.cn (C.C.); lishi182@163.com (Y.H.); 383018017@qq.com (P.X.)

[3] School of Mechanical Engineering and Automation, Northeastern University, Shenyang 110819, China

* Corresponding author. E-mail: maliang7653@sina.com (L.M.); suncong1@mail.neu.edu.cn (C.S.)

Received: 5 January 2025; Accepted: 18 March 2025; Available online: 24 March 2025

ABSTRACT: Shear stress prediction in high-concentration magnetorheological fluids (MRFs) faces limitations due to the oversimplified magnetic dipole interactions and neglect of multibody effects in classical single-chain models, particularly under conditions (30–40 vol.%) where stress prediction errors start escalating nonlinearly. To address this gap, based on the classic single-chain model, this study proposed a new revised calculation method that integrates three novel components: (1) a distance-weighted dipole interaction model incorporating material-specific correction factors, (2) dynamic chain reconstruction mechanisms accounting for magnetic aggregation under shear deformation, and (3) transverse field overlap parameters quantifying anisotropic field distributions. Validated against Lord Corp.'s MRF-132DG, the proposed approach reduces shear stress prediction root-mean-square error (RMSE) by 71.7% (from 27.40 kPa to 7.76 kPa). It rectifies the R-square metric from −0.9236 to 0.8457, outperforming existing models in high-concentration regimes. The work resolves the bottleneck of modeling chain-to-network transition behaviors through Monte Carlo simulations with energy barrier analysis, revealing how localized dipole rearrangement governs macroscopic rheological responses. The methodology's adaptability to pre-saturation magnetization stages further enables systematic evaluation of multi-dipole interaction thresholds critical for high-performance MRF engineering applications.

Keywords: Magnetorheological fluid; Shear stress microscopic model; Magnetically-induced polarization force; Magnetic chain

1. Introduction

Magnetorheological fluids (MRFs) are intelligent materials composed of magnetic particles, base carrier fluid and additives [1]. They are widely applied in fields including damping and shock absorption [2–6], power transmission [7,8], supporting systems [9,10], precision medical devices [11–14], and polishing processing [15,16]. When an external magnetic field is applied to the magnetorheological polishing fluid, a Bingham plastic body with anisotropic multi-chain aggregation will be formed rapidly [17]. Its shear stress is $10^2 \sim 10^5$ times higher than in a zero magnetic field environment [18]. By taking advantage of this property, the magnetorheological polishing fluid, through the control and modulation of the external magnetic field to trigger the rheological effect, has the capacity to realize deterministic polishing [19–21]. This process can achieve a surface figure accuracy of PV < 50 nm and a surface roughness R_q of less than 1 nm, all while scarcely generating subsurface damage [22–24]. However, one of the prerequisites for realizing this deterministic magnetorheological polishing process is to accurately evaluate the force-magnetic coupling behavior of the magnetically induced multi-chain aggregated microstructures when the magnetic particles with different volume fractions undergo the rheological effect [25–27].

The fundamental reason for the occurrence of the rheological effect in magnetorheological fluids (MRFs) lies in the polarization of the magnetic particles inside MRFs, which is induced by the external magnetic field. Scholars have conducted a series of studies on the relationship between the microstructure and the magnetic field force of

https://doi.org/10.70322/ism.2025.10009

magnetorheological fluids in which the rheological effect has occurred. Based on Maxwell's equations and the fixed dipole assumption that ignores the locally induced magnetic field of each magnetic particle itself, Rosensweig [28] established the generalized expression in the microscopic form of the fixed dipole magnetic field force acting on the particle under the action of the external field strength, as shown in Equation (1), that is, fixed dipole model (FDM). FDM expresses the resultant magnetic field force acting on the particle i at position $\mathbf{Y}^{(i)}$ by all N particles with magnetic dipole moments of $\mathbf{m}$ the magnetorheological fluid to which an external magnetic field is applied.

$$\mathbf{F}^{(i)} = \mu_0 \nabla(\mathbf{m} \cdot \mathbf{H}) = \mu_0 \nabla_{\mathbf{Y}^{(i)}} \left[\mathbf{m} \cdot \sum_{k=1,k\neq i}^{N} \mathbf{H}_{\text{dipole}} \left(\mathbf{Y}^{(i)} - \mathbf{Y}^{(k)} \right) \right] \tag{1}$$

Furthermore, assuming that the overlay effect of the dipole excitation magnetic field itself is taken into account, by replacing $\mathbf{m}$ in the expression with the point dipole moment $\mathbf{m}^{(i)}$ shown in Equation (2), the mutual dipole model (MDM): $\mathbf{F}^{(i)} = \mu_0 \nabla(\mathbf{m}^{(i)} \cdot \mathbf{H})$, can be constructed.

$$\mathbf{m}^{(i)} = \frac{4}{3}\pi R^3 \frac{3\chi}{\chi + 3} \cdot \left[\mathbf{H}_0 + \sum_{k=1,k\neq i}^{N} \mathbf{H}_{\text{dipole}} \left(\mathbf{Y}^{(i)} - \mathbf{Y}^{(k)} \right) \right] \tag{2}$$

Since the MDM considers the local magnetic field of particles, by comparing the R^2 values of the measured F / μ_0 data, it has been verified that, compared with the FDM, the predicted values of the MDM are more consistent with the experimental results of the magneto-induced rheological effect of MR fluid [29].

The MDM explains why MRFs (Magnetorheological Fluids) can switch between fluid and solid states within an extremely short period of time after an external magnetic field is applied and simultaneously exhibit an obvious transformation in mechanical properties characteristic of non-Newtonian fluids. Nevertheless, in the scenario where the volume concentration of particles in magnetorheological fluids is relatively high, the number and distribution of dipoles in the system will significantly increase the complexity of the model. Some recent research efforts have verified the relationship between the shear modulus of magnetorheological elastomers and the magnetically induced interaction energy through the finite element method [30]. Drawing on the dipole theory, Jang [31] incorporated the particle interaction within parallel plates under the influence of an external magnetic field and proposed a three-dimensional microscopic computational model for shear stress. By means of the Leknar summation algorithm, the effect of the magnetically induced force of dipoles was evaluated, expediting the convergence rate of the model. However, given the complexity of the particle interaction transformation function form in the Leknar algorithm, its dissemination in engineering applications might present an obstacle.

Therefore, some other studies have been devoted to simplifying the assumed forms of the magnetic chain microstructure and analyzing the impacts of these specific structures on the macroscopic mechanical properties under the action of the rheological effect. Some works [32,33] assumed the multi-chain aggregated structures of magnetic particles to be different idealized structural forms, such as infinitely long single chains, closely packed double chains, and cylinders, respectively. Tang [34], on the other hand, abstracted the magnetorheological fluid in the state of rheological effect as a two-dimensional plate-like structure for analysis. The above work constructed models corresponding to different structural form assumptions. The controlled magnetic particles in the corresponding magnetic chain structures generate corresponding microscopic magnetic field forces under the combined action of magnetically induced polarization energy, van der Waals potential energy, and steric hindrance energy. Moreover, the inherent mathematical relationships between the magnetic field force and key parameters, such as the external magnetic field intensity, the particle spacing, and permeability, were elaborated.

The results of subsequent, more in-depth research have shown no simple linear correlation between the microscopic magnetic chain structure and the volume fraction of magnetic particles in magnetorheological fluids. Zhu et al. prepared four dimethyl silicone oil-based magnetorheological fluids (MRFs) with volume fractions ranging from 10% to 40%. Rheological tests on their magnetic field-induced shear characteristics revealed that the magnetic particles within the MRFs transitioned from disordered distributions to dense chain or network structures under magnetic fields, strengthening interparticle magnetic interactions [35]. This structural evolution resulted in a 3–4 fold enhancement in shear resistance within the shear rate range of 300–800 s^{-1} under equivalent conditions. Separately, Sarkar et al. [36] experimentally investigated shear resistance by comparing three volume fractions (9%, 18%, and 36%) in self-prepared silicone oil-based MRFs (with oleic acid additives). Their orthogonal experiments employed spherical small iron particles (μm, mean size $\mu = 9.27$, variance $\sigma^2 = 4.63$) and large flaky particles (μm, $\mu = 120.85$, $\sigma^2 = 56.05$), testing configurations of pure small particles, pure large particles, and a 50:50 particle mixture. Their results similarly

confirmed that higher-volume-fraction MRFs exhibit superior shear resistance but are more prone to sedimentation. These parallel findings from both investigations underscore the critical necessity of studying the shear rheological properties of high-volume-fraction MRFs.

The microstructural discrepancies among magnetorheological fluids (MRFs) with varying volume fractions lead to computational discrepancies when employing different structural modeling hypotheses, where distinct modeling assumptions induce prediction errors of differing magnitudes. Some scholars have conducted a comparative analysis of the theoretical shear yield stress when magnetic particles reach saturation magnetization under different volume fractions, considering both the single-chain model and the columnar structure model. It was found that when the particle volume fraction gradually increases and exceeds 30%, the error between the results calculated based on the columnar and single-chain models has always remained at a level of more than 15% [37]. If the volume concentration of particles is continuously augmented, the calculation error will also exhibit a tendency to increase in accordance with the mathematical principle of the quadratic power law. The two-dimensional plate-like structure shear stress model proposed by Tang takes into account the integrity of the rheological structure. During the model construction process, it is essential to consider the anisotropic characteristics that manifest themselves during particle magnetization.

Constructing a simple yet versatile microscopic shear model of chain-like structures is essential for understanding the connection between the dynamic evolution of magnetic chain formation and macroscopic shear rheological properties. In the numerical simulation of particle ensembles within magnetorheological systems using the Monte Carlo method [38,39], the probabilistic impact of minor trial displacements on global system energy variation is evaluated. Recognizing that previous studies have highlighted the significant influence of magnetic particle volume fraction on the shear mechanical behavior of magnetorheological fluids, this study extends these findings by employing Monte Carlo simulations to obtain spatial coordinates and magnetic moment orientations of all particles within the system. Particle positions within magnetic chains are evaluated based on simulated configurations and magnetic alignment data. By incorporating distance parameters and material adjustment factors, an enhanced microscopic model is established that characterizes shear stress variations in magnetorheological fluids with high particle concentrations (approximately 40 vol.%).

2. Microscopic Model of Single-Chain Shear Stress

The accuracy of shear stress modeling in magnetorheological fluids (MRFs) fundamentally depends on the precise characterization of magnetic chain behavior. This section systematically evaluates the framework and limitations of the classical single-chain model through theoretical analysis and quantitative validation.

The single-chain shear stress model (in Equation (3)) proposed by Ginder expresses the shear force per unit area within a specified domain of particles that have been affected by magnetic field polarization on a single magnetic chain. In Equation (3): $\gamma = \tan\omega$ represents the shear strain rate, and F is the horizontal tangential force between magnetic particles.

$$\tau = \frac{\gamma}{1+\gamma^2} \cdot \frac{4F}{D^2} \tag{3}$$

When a horizontal force is applied to the particles, as shown in Figure 1, the particles move from the position indicated by the dotted line to the position of the point O_i. The shear angle between the particles is ω, and the center distance expands from the original h to $h/\cos\omega$. The magnetic field application range of any magnetic particle on the magnetic chain is defined as a hexahedron with $V = D^2 h$, where λ_h and λ_D are conversion coefficients related to the particle radius.

Ginder's model assumes that each magnetic chain in the magnetorheological fluid is independent and not affected by the additional magnetic fields of other magnetic chains, and that each particle on the chain is polarized only under the action of the external field. This presumption substantially reduces the computational complexity involved in the model. Some studies [29] also indicate that in the calculation results of the single-chain model, the error between the particle volume concentration and the parameter F/μ_0 is correlated in accordance with the quadratic power law. The results obtained under the condition of low volume fraction are in agreement with the experiments.

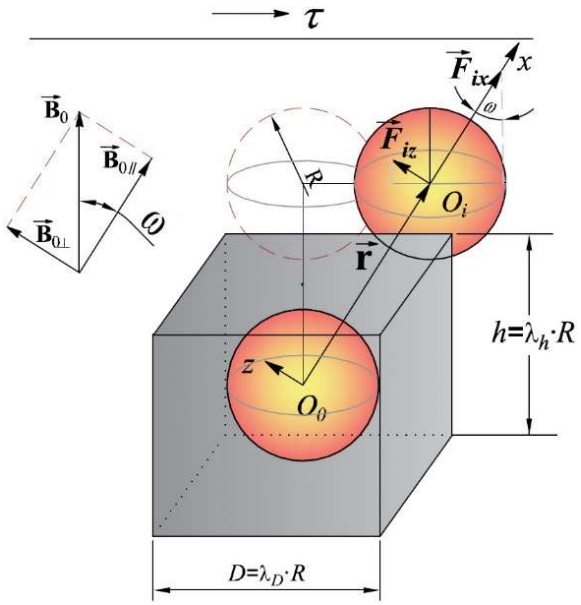

Figure 1. Force Analysis of Rheological Shear Stress in Magnetorheological Fluid Induced by External Magnetic Field.

2.1. Evaluation of the Accuracy of the Single-Chain Shear Stress Model

Sedimentation characteristics represent one of the fundamental properties governing the functional performance of magnetorheological (MR) fluids. Key factors affecting their stability include operating temperature, density differences between carrier fluids and particles, and MR fluid volume fraction [40]. In the evaluation of the current simulation model, the focus lies on shear resistance properties under effective working conditions. At the same time, the influence of the size of ellipsoid-like particles on the structural anisotropy of the simulation is negligible [41]. Hence, the following assumptions are made: (1) optimal ratios of dispersants and stabilizers are ensured; (2) all particles are spherical with identical diameters and uniformly dispersed within the MR fluid system. In the improved model proposed in the subsequent discussion of this paper, the same set of model assumptions—including uniform particle dispersion, identical spherical geometry, and optimized stabilizer parameters—will be retained.

When applying Ginder's single-chain model to estimate shear stress dependence on particle volume fraction φ, additional considerations must account for (i) the thickness of the stabilizer layer surrounding magnetic particles and (ii) geometric alignment patterns of magnetic chains.

According to the geometric volume equivalence relationship between spherical particles and the hexahedral action domain, the height and width distance coefficients λ_h, λ_D and the volume fraction ϕ satisfy the following formula:

$$\lambda_h \lambda_D^2 = 4\pi / 3\phi \tag{4}$$

In consideration of the thickness of the outer stabilizing agent layer of magnetic particles, it is postulated that adjacent particles on the magnetic chain are enwrapped with a stabilizing agent layer of approximately $\delta \approx 0.1R$. Concurrently, it is requisite to guarantee that the magnetic field polarization effect does not attenuate owing to overly long distances between particles. The "proximity" range of the distances between particles is defined as presented in Equation (5) [42].

$$[r_{i,j}^{\min}, r_{i,j}^{\max}] = (2.2 \sim 2.4)R \tag{5}$$

Assume that the outer stabilizing agent layers will not penetrate into each other. Then, in Equation (5), when $\lambda_h = \lambda_D = 2.2$, the theoretical volume concentration limit of the magnetorheological fluid with magnetic chains arranged parallel to the external magnetic field and with uniform particle radii is $\phi_{\max} = 39.34\%$. If this concentration continues to increase, it will lead to an overlap of the local magnetic field action regions between different magnetic chains, and the error in calculating the shear stress of the magnetorheological fluid using the single-chain model will increase rapidly. However, considering factors such as the irregular arrangement of particles in the zero field, the dynamic arrangement of magnetic chains being affected by sedimentation and inertial forces, and the existence of unequal angles between the magnetic moment of particles and the direction vector of the external magnetic field, the volume fraction threshold at which the local magnetic field action regions of particles overlap is significantly smaller than $\phi_{\max}$.

As shown in Figure 2, scanning electron microscopy (SEM) analysis of the magnetorheological fluid under zero magnetic field conditions reveals distinct morphological features. The iron powder particles exhibit a uniform average size of approximately 2 μm, displaying minimal aggregation and debris formation while maintaining well-dispersed flocculent-stabilized surfaces. This structural consistency aligns with Monte Carlo simulation results for low-concentration systems (applied parameters: B = 0.2 T, d = 2 μm, 10 vol.%, as described in Section 3.2), where initial particle aggregation tendencies are observable under external fields.

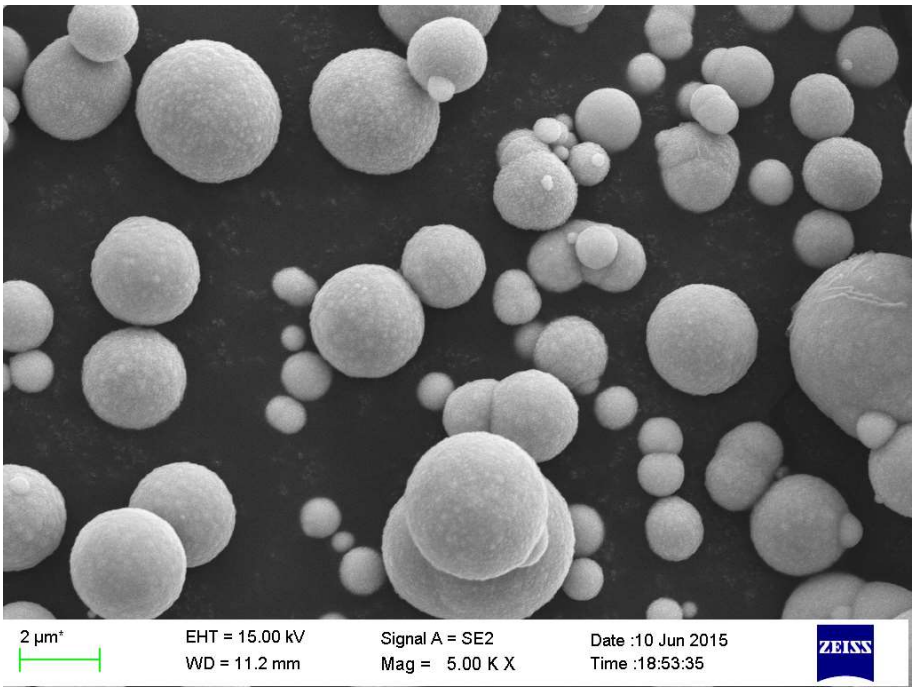

Figure 2. SEM image of MR fluids sample (5Kx, 2 μm).

2.2. Impact of Magnetic Particle Volume Fraction

After an external magnetic field is applied, changing the volume fraction ϕ, is equivalent to altering the spacing between magnetic chains. When its value is lower than ϕ^{lim} (a relatively small proportion), as presented in Figure 3a, the magnetic chains within the magnetorheological fluids (MRFs) exhibit a dispersed state. They are predominantly oriented along the direction perpendicular to the externally applied magnetic field. The increase in shear force caused by the overlap of magnetic fields among different magnetic chains in the cross-section is negligible. Under such circumstances, applying the infinite long single-chain structure to evaluate the shear stress of the magnetorheological fluid will be closer to the calculation results of the model itself [43].

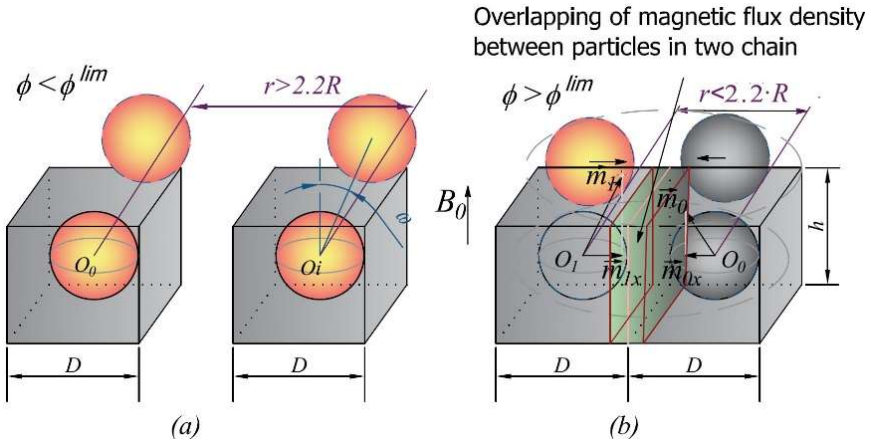

Figure 3. Comparison of chains-to-chain interaction effect with different volume fraction. (**a**) Large lateral spacing of adjacent flux chains vs. particle local field area; (**b**) Overlapping transverse magnetic field areas of particles in flux chains.

With the augmentation of the particle volume fraction in the magnetorheological fluid, the inter-magnetic-chain spacing within the carrier fluid initiates a gradual reduction, and the local magnetic fields of distinct magnetic chains commence to overlap, as depicted in Figure 3b. This is equivalent to the situation where the magnetic chains that should have been distributed over a larger transverse acting area are now deployed on a smaller cross-section, intensifying the transverse interaction effects among the magnetic chains. As a result, when the classic single-chain model is employed to compute the shear stress, the obtained values are beneath those of the experimental data. To estimate the accuracy of the polarization force generated due to the aggregation of multiple chains, some researchers have proposed introducing distribution functions to calculate the number of magnetic chains and to statistically analyze the superimposed contribution rate of chains to the horizontal shear stress per unit area [44]. This method enables the calculation of the number of chains on the cross-section. However, the accuracy of estimating the distribution characteristics of the angles between magnetic chains and the external magnetic field depends on the samples of shear stress results obtained during the preparation and testing of MRFs.

Another approach for estimating the influence of the overlap of magnetic fields is to, based on the dipole theory, establish the local magnetic field expression $\mathbf{B}_P$ between any adjacent particles O_0 and O_i on a magnetic chain in the direction of the external magnetic field $\mathbf{B}_0$, and represent it as the integral of the magnetic dipole moment $\mathbf{m}_0$ of particle O_0 with respect to the induced intensity on particle i:

$$\mathbf{B}_P = \int \mathrm{d}\mathbf{B}_P = \frac{\mu_f}{4\pi}\int\left(\frac{3\mathbf{m}_0\cdot\mathbf{r}}{r^5}\cdot\mathbf{r}-\frac{\mathbf{m}_0}{r^3}\right) \tag{6}$$

In Equation (6), μ_f represents the magnetic permeability of the carrier fluid, which can be approximated by the vacuum magnetic permeability $\mu_0 = \mu_f = 4\pi\times10^{-7}$ H/m. $\mathbf{r}$ represents the vector pointing from the center of the magnetic dipole $\mathbf{m}_0$ to point P on O_i. According to Ampère's law, within the action region Ω of the particle, the infinitesimal length of the magnetization current is integrated over the action domain to obtain the particle polarization force $\mathbf{F}_i$.

$$\mathbf{F}_i = \iint_\Omega I\mathrm{d}l_i \times \int_0^\pi \left(\mathrm{d}\mathbf{B}_{P\square} + \mathrm{d}\mathbf{B}_{P\perp}\right) = [\mathbf{F}_{ix}, 0, \mathbf{F}_{iz}] \tag{7}$$

In Equation (7), $\mathbf{F}_{ix}$ and $\mathbf{F}_{iz}$ are the values determined by the numerical integral expression of the magnetic induction intensity $\mathbf{B}_P$ of the particles. By combining Equations (3)–(7), the calculation expression for the shear stress of the single-chain model on the cross-section D^2 can be obtained as Equation (8), which is proportional to the square of the magnetization intensity M of the particles.

$$\tau = \frac{F_\kappa}{D^2} = \frac{-\mathbf{F}_{iz}\sin\omega + \mathbf{F}_{ix}\cos\omega}{D^2} = \frac{3\lambda_h\kappa(\lambda_h,\omega)}{4\pi}\cdot\mu_f\phi\cdot M^2 \tag{8}$$

Equation (8) is the microscopic calculation model for the shear stress of a single magnetic chain under an external field, and it is related to both the particle spacing coefficient and the particle magnetization intensity parameter. The particle magnetization intensity in the equation can be simulated by using the Fröelich-Kennelly material model [45], as shown in Equation (9) to model the nonlinear magnetization behavior of particles in the external magnetic field. The material susceptibility of ferromagnetic particles is taken as $\chi_0 = 1000$.

$$M = H(B)\cdot\frac{(\chi_0-1)M_s}{(\chi_0-1)+M_s/H(B)} \tag{9}$$

The parameter $\kappa(\lambda_h,\omega)$ in Equation (8) related to the distance coefficient λ_h and the shear angle ω is shown in Equation (10). $f_x(\lambda_h,\omega)$ and $f_z(\lambda_h,\omega)$ are coefficients that need to be integrated. Their integrand expressions are the cross products of the infinitesimal current elements and the magnetic fields of the particles, and the results can be calculated by means of numerical integration methods.

$$\kappa(\lambda_h,\omega) = \sin^2\omega f_x(\lambda_h,\omega)\cos\omega + \left(\frac{8\pi\sin\omega\cos^2\omega}{3\left[-1+(\lambda_h/\cos\omega)^2\right]^2} - \sin^3\omega f_z(\lambda_h,\omega)\right) \tag{10}$$

2.3. Results of the Single-Chain Model and Evaluation

The microscopic model within the framework of the single-chain theory does not fully concentrate on enumerating the quantity of magnetic chains in accordance with the volume fraction of magnetic particles. Instead, it derives the contribution of the shear stress of a single magnetic chain. Therefore, it differs from the approach adopted in Reference [46], which corrects and calculates the shear force using the probability distribution function. Moreover, it does not take into account the transverse influence caused by the overlap of the effective magnetic field regions of magnetic chains due to the aggregation and entanglement of magnetic chains on the same cross-section under the condition of high volume fraction. If the shear stress of the magnetorheological fluid is calculated according to this model, its theoretical value will be smaller than the experimental value before the magnetic chain particles reach the saturation magnetization intensity.

Figure 4 illustrates the $\tau - B$ result curves computed via the single-chain model under the circumstances where the volume fraction ϕ is set at 20%, and the relative magnetic permeability μ_r of the ferromagnetic material of the particles is 1000, with the magnetic field intensity being subject to variation. Within the range of magnetic induction intensity where $0 \le B \le 3\mathrm{T}$, when the magnetic induction intensity of the ferromagnetic particles in the magnetorheological fluid reaches saturation, the shear stress begins to approach a stable state and no longer increases with the external magnetic field. The saturation magnetization intensities of the three curves are 1.0 T, 1.5 T, and 2.0 T, and the corresponding shear yield stresses are 10.94 kPa, 24.58 kPa, and 43.62 kPa respectively, showing a roughly quadratic power-law growth. This indicates that improving the magnetic quality factor of the particles can effectively enhance the rheological mechanical properties of the magnetorheological fluid.

In Figure 5, while keeping the saturation magnetization intensity M_s of the particles unchanged, the curves of the shear yield stress of MRFs with different volume fractions varying with the external magnetic field intensity. The results verify that the variation of $\tau(\phi) - B$ increases in an approximately linear pattern according to the single-chain model.

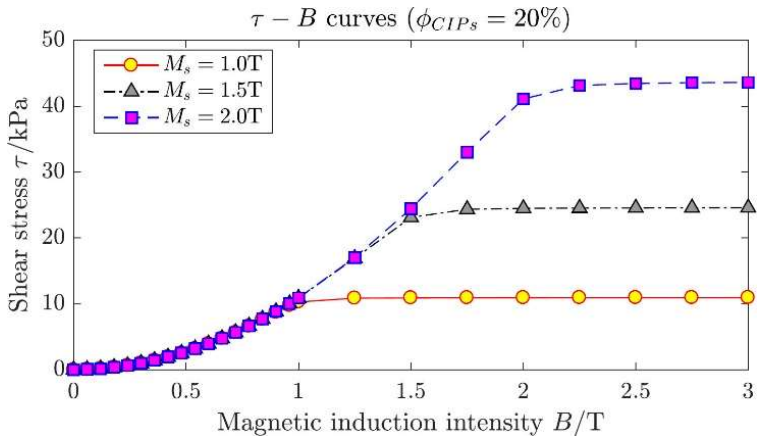

Figure 4. $\tau - B$ Curves with Particle M_s.

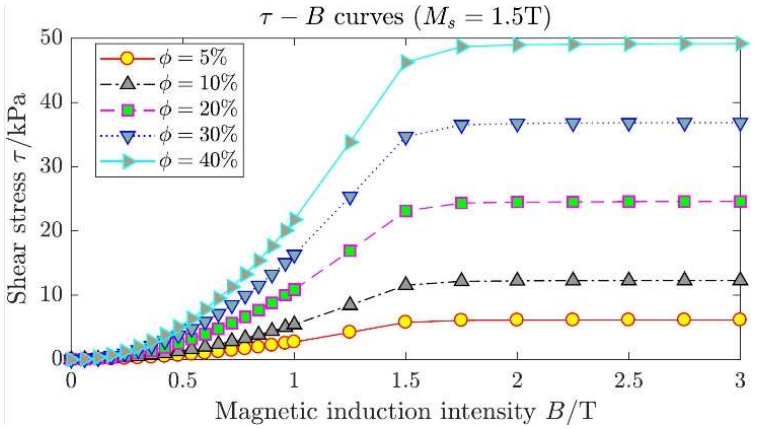

Figure 5. $\tau - B$ Curves with Vol.%.

3. Distance-Weighed Single-Chain Shear Stress Model

The classical single-chain model significantly underestimates shear stress values in high-volume-fraction magnetorheological fluids (MRFs) due to its inherent neglect of transverse magnetic interactions between overlapping chains. To address this limitation, this section proposes a revised microscopic model that incorporates distance-weighted parameters to capture the amplification effect arising from aggregated magnetic chains. By integrating Monte Carlo simulation-derived coefficients—weighting both interparticle distance and material properties—the revised model dynamically adjusts chain spacing and polarization forces under varying volume fractions.

3.1. Increment Coefficient of Magnetization Intensity

A weighted amplification coefficient A_M is introduced into the simulation model to evaluate the degree of overlap of the transverse magnetic field intensity resulting from the aggregation of multiple magnetic chains, as shown in Equation (11). This coefficient is associated with the total number of particles N in the simulation system, the average number of particles $\bar{k}_n$ on the effective magnetic chains within the system, the tentative coefficient β related to the magnetization properties of ferromagnetic particles, and the particle volume fraction ϕ of the magnetorheological fluid.

$$A_M = \left(N / \bar{k}_n\right)^{\beta\phi} \tag{11}$$

3.2. Validity of Magnetic Chains

During execution of the Monte Carlo simulation, $\{[x_i, y_i, z_i], [m_{xi}, m_{yi}, m_{zi}]\}$, *i.e.*, the configuration matrix $\mathbf{P}$, which incorporates the positional and orientational particulars of all particles, experiences modifications within each iterative cycle [47]. As the simulation advances, the particle system progressively manifests the characteristics wherein the directions of magnetic moments on the magnetic chains tend towards alignment, and multiple chains coalesce. The Monte Carlo simulation results of the magnetorheological system presented below illustrate four existing forms of magnetic chains.

When simulating the dynamic structural evolution of magnetic chains in magnetorheological fluids using the Monte Carlo method, determining whether any two particles in the system are adjacent within the same magnetic chain involves two criteria beyond geometric proximity (as expressed in Equation (5)): the polarized attraction between neighboring particles on the chain and the magnetostatic interaction energy from the local magnetic field. These dual criteria are visually presented in Figure 6b–e, where arrows indicate the magnetic moment orientations of particles at the end of each iteration. It is evident that for sufficiently close adjacent particles sharing a magnetic chain, the angle between their magnetic moments must also be sufficiently small.

According to Reference [48], two adjacent particles are considered to belong to the same magnetic chain if the angle between the vector connecting their centers and the direction of the external magnetic field is less than $\arccos\sqrt{5}/5$. These particles are subsequently grouped into distinct chain sets and excluded from further iterations. In contrast, the chain configuration in Figure 6e is deemed invalid due to noncompliant angular criteria. During Monte Carlo simulations, such particles continue to undergo random displacement trials in subsequent iterations, gradually migrating to other valid chains until the iteration process concludes.

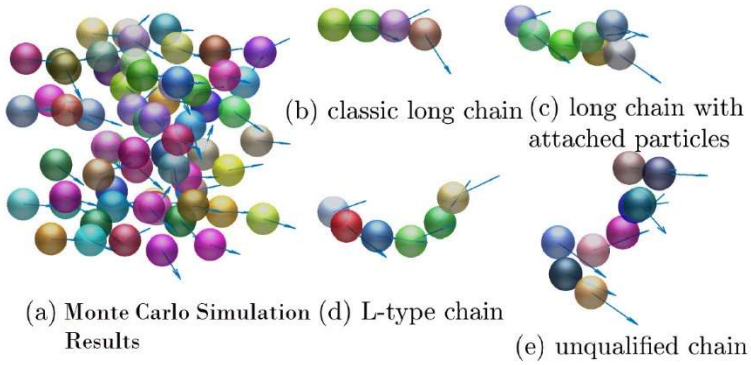

Figure 6. Dynamic Evolution of Magnetic Chains in MRF Under Magnetic Field via Monte Carlo Simulation.

3.3. Shear Stress Correction Calculation Model

The operations to assemble a collection of valid magnetic chains in the concluding state subsystem of the Monte Carlo simulation are enumerated as follows:

1. In the nth iteration, iteratively process the particle number index k_{nl}, and search for k_{ni} that meets the center distance requirement in the state configuration matrix $\mathbf{P}_n$ until there are no particles in the system that satisfy the adjacent condition anymore;
2. Calculate whether the average value of the angles between the vectors of the center-to-center distances of adjacent particles in the particle set and the external magnetic field is less than $\arccos(\sqrt{5}/5)$. If so, this set of particles forms a magnetic chain $C_{kn}^{(i)}$;
3. Execute Step 1 and Step 2 to iteratively process all the particles within the system, thereby generating the set of valid magnetic chains $\left\{C_k^i\right\}$.
4. Calculate the mean value of the number of particles on the valid magnetic chains according to Equation (12)

$$\overline{k}_n = \sum_{i=1}^{n} \frac{k_{ni}}{n} \tag{12}$$

In the set of valid magnetic chains, calculate the weighted distance coefficients $\left\{\overline{\lambda}_{Ckn}^i\right\}, \forall i = 1,\ldots,n$ among k_{ni} particles on n magnetic chains according to Equation (13). Use this value to replace the magnetic chain particle spacing coefficient λ_h (see Equation (10))

$$\overline{\lambda}_{Ckn}^i = 2\frac{\sum_{t=1}^{kn} \lambda_{Ckn(t)}^{(i)}}{d} \tag{13}$$

By integrating Equation (8) with Equations (11)–(13), a novel and revised microscopic model for shear stress, which is presented as Equation (14), is derived. The new model adjusts the shear stress by modifying the mean number of particles k_n on the valid magnetic chains and the spacing coefficient λ_n, so as to obtain stress results that are closer to those of the actual MRFs.

$$\overline{\tau} = \frac{1}{n}\sum_{i=1}^{n} \tau^{(n)} = \frac{3\left(A_M \cdot M\right)^2}{4\pi n} \cdot \sum_{i=1}^{n}\left[\overline{\lambda}_{Ckn}^{(i)} \cdot \kappa\left(\overline{\lambda}_{Ckn}^{(i)}, \omega\right)\right] \tag{14}$$

4. Validation

Comprehensive validation is critical to establish the predictive superiority of the revised distance-weighted model over classical approaches. This section employs experimental data from Lord Corporation's MRF-132DG magnetorheological fluid (material parameters in Table 1) to evaluate two key parameters: the modified spacing coefficient (accounting for interchain interactions) and the adjusted particle population distribution on active magnetic chains. Through quantitative benchmarking, we demonstrate how these corrections align theoretical predictions with empirical observations.

Table 1. MRF-132DG: Material Parameters.

Parameters	ϕ_m / wt.%	ρ / g·cm^{-3}	ϕ / vol.%	M / T
Value	80.98	2.95~3.15	39.57	1.4071

4.1. Spacing Coefficient and Magnetic Field Amplitude Coefficient

The MRF-132DG type magnetorheological fluid, whose material parameters are shown in Table 1, sourced from Lord Company, is chosen as the reference specimen [49].

By inputting the four sets of magnetorheological fluid material parameters listed in Table 1 and run the Monte Carlo simulation program, the distance-weight coefficients k_n and λ_{Ckn} were obtained. Regarding the expression of the shear stress model in Equation (14) as a function with respect to the magnetic flux density B, denoted as $\tau(B)$, the task of determining the adjustment coefficient β is then converted into the problem of seeking the nonlinear least-

squares solution for the exponent β in light of the available data pairs (B,τ). Ultimately, by substituting k_n, λ_h and β into Equation (14), the calculated values of the distance-weight factor A_M were acquired. The aforesaid results are presented in Table 2.

Table 2. Simulation and Calculation Results.

H **(KA/m)**	**82**	**142**	**186**	**220**	**250**
k_n	5.31	4.23	4.25	5.44	5.11
λ_h	2.2166	2.2268	2.2364	2.2193	2.1894
β	0.6072	0.6230	0.6345	0.6014	0.6109
A_M	1.8334	1.9378	1.9356	1.8226	1.8506

Upon analyzing the result data in Table 2, it is found that the changes in the coefficients k_n, λ_h, and β with the variation of the external magnetic field intensity are minimal. It is considered that the primary reason for this situation is that for MRFs with a high-volume percentage, the spacing between magnetic chains is rather small, imposing more restrictions on the free movement of particles. At this point, the interaction forces between particles reach the critical value even when the external magnetic field value is relatively low. Therefore, the average values of the three coefficients under different external magnetic field intensities are taken, specifically: $\overline{\lambda_h} = 2.177$, $\overline{k_n} = 4.868$, and $\overline{\beta} = 0.6154$, to calculate the gain weight factor A_M.

4.2. Comparison between Simulation Model and Experimental Data

Evaluate the shear stress as a function of magnetic flux density, $\tau(B)$, utilizing two distinct shear stress models, namely Equation (10) and Equation (14), with the parameters specified on the product page of the MRF-132DG type magnetorheological fluid (refer to Table 2). The comparison outcomes between the computational results of the two models and the rheological experimental data are presented in Figure 7.

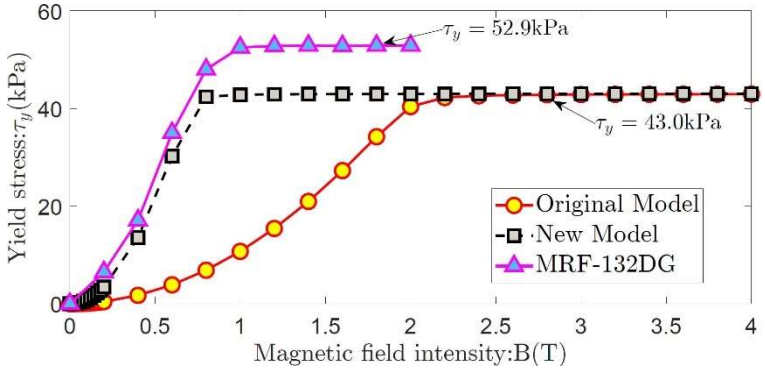

Figure 7. Comparison of Shear Stress Results of Two Models and Experimental Data of MRFs-132DG.

In Figure 7, "Original Model (●)" represents the classical single-chain shear stress model (see in Equation (10)), while the "New Model (■)" represents the calculated values obtained according to the distance-weighted shear stress model (Equation (14)). When compared with the experimental data (▲) of MRF-132DG, it can be found that as the intensity of the external magnetic field increases:

- In the initial stage when the applied external magnetic field has not reached the magnetization saturation intensity of the particles, the growth rate of shear stress in the original model is significantly lower than the result data of the rheological experiment. The stress steady-state stage is not entered until $B \approx 2.2\text{T}$;
- In the initial stage, where the applied external magnetic field has not reached the magnetization saturation intensity of the particles, the growth rate of the shear-stress model corrected by distance-weight is basically consistent with the experimental data. The steady-state stage is reached when the external magnetic field is 1.0T;
- After reaching the magnetization saturation intensity of the particles, when comparing the calculated shear-stress results of the classical single-chain model and the new distance-weight model, the two are basically consistent (43.0 kPa). However, this predicted stress value is lower than the corresponding experimental data value (52.9 kPa).

It can be seen from the results of the three curves that the shear stress varying with the external field, which is calculated according to the new model (■), is more in line with the actual experimental data. This confirms that the overlap of transverse magnetic fields among the magnetic chains amplifies the shear stress generated after particle

polarization. However, the distance-weighted model is rather conservative in calculating the steady-state value of the shear yield stress. This may be due to the deviation between the assumption of the particle spacing and the actual situation. In the Monte Carlo simulation, in order to simplify the calculation, it is assumed that the spacing range of the particles on the magnetic chains is 2.2 to 2.4 times the radius. However, under the action of the external field, especially under the effect of a strong magnetic field, the stabilizing agent layers covering the adjacent particles will be squeezed and deformed to different extents due to the polarization effect (the stronger the magnetic field, the more obvious the deformation). The actual particle spacing is less than 2.2 before the model is modified. Therefore, the original assumption of the spacing underestimates the actual interaction force on the magnetic chains.

4.3. Impact of Simulation Parameters on Stress Results

The novel and revised microscopic model of distance-weighted shear stress simulates the variation in shear stress, which is induced by the overlap of magnetic fields between chains due to the increase in volume fraction, through the introduction of distance-weighted parameters k_n and λ_h. Subsequently, the influence of these two factors on the generation of shear stress is analyzed.

Assume that the volume concentration of ferromagnetic particles in self-prepared magnetorheological fluid is 38.7%, and the shear yield stress is observed near a particle magnetic induction of B = 1.2 T. With the magnetic induction held constant at this value, the variation of shear yield stress with the particle distance weighting coefficient is plotted, as shown in Figure 8. Here, the gray shaded region indicates that as the distance coefficient increases from 2.2 to 2.4, the shear yield stress decreases from 40.66 kPa to 29.7 kPa. The asterisk (★) denotes the experimentally measured shear yield stress values.

In Figure 8, the relationship between the parameters τ_y and λ_h depicted by the curve cannot be measured via physical experiments. However, this set of results can reveal that the attenuation effect of the polarization force of magnetic particles, as the inter-particle distance increases, approximately exhibits a decline following a quadratic power-law. When the thickness of the outer coating increases from 10% to 20%, the shear-yield stress calculated by the model shows a reduction of approximately 27.0%. This alteration indirectly validates that the distance coefficient can be utilized to assess the variations in the micro-mechanical properties of the magnetorheological fluid.

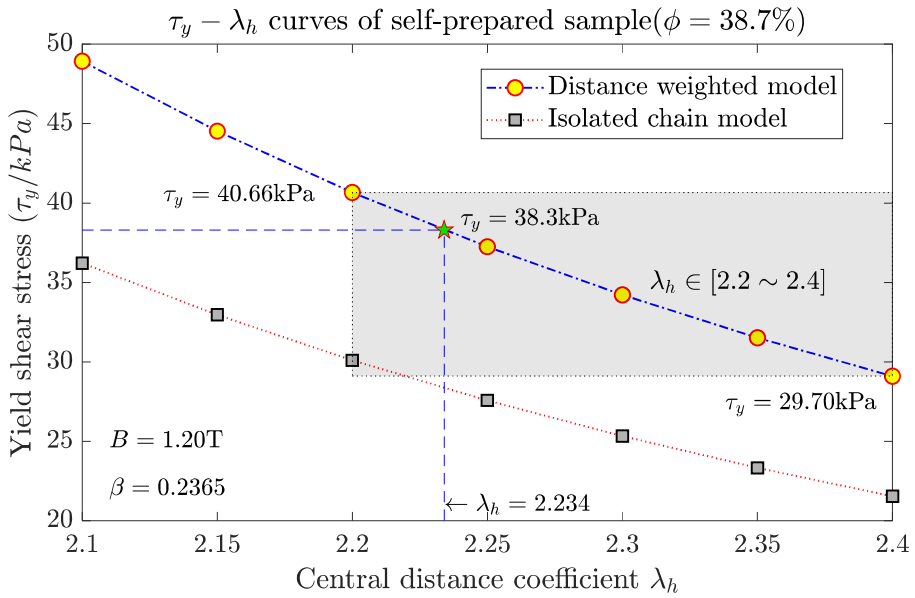

Figure 8. Curves of Distance Simulation Parameter on the Calculated Values of the Shear Stress Model.

The adjustment coefficient β is the least-squares solution obtained from the expression of the distance-weight model based on the $B-\tau$ data in the rheological experiments. This parameter is related to the magnetic flux density B of the particles, the distance-weight coefficient λ_h, and the volume fraction ϕ. The more accurate the experimentally measured $\tau(B)$ data are, the more reasonable the evaluation of the ferromagnetic particle material properties by β will be. Figure 9 plots the simulated shear yield stress curve (represented by a circle-marked dash-dot line, under the condition of $B = 1.2\text{T}$ and $\lambda_h = 2.234$), as a function of the material adjustment coefficient β. It can be observed that the shear yield stress increases rapidly when β ranges from 0.1 to 0.4. As β continues to increase beyond this

range, the shear stress stabilizes, indicating that the influence of the material adjustment parameter β on the shear stress in the model does not follow a linear variation pattern.

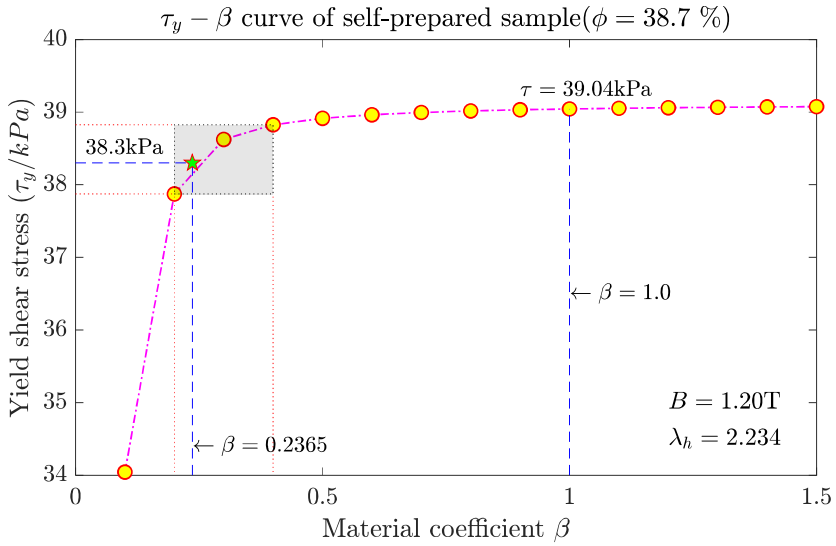

Figure 9. Curve of Material Property Simulation Parameter on the Calculated Values of the Shear Stress Model.

When the simulation program calculates the adjustment coefficient of this magnetorheological fluid to be $\beta = 0.2365$, the corresponding shear yield stress value is 38.3 kPa (As shown in the position of "★" in the Figure 9), which is clearly lower than the calculated value (43.0 kPa) of the MRF—132DG magnetorheological fluid model with a similar volume fraction (39.57%) but a different adjustment coefficient ($\beta_{132DG} = 0.6154$), or the experimentally measured data (52.9 kPa). Although the ϕ parameter values of the two magnetorheological fluids are close, there are significant differences in their shear yield stresses. This confirms that there is a connection between the adjustment coefficient β and the material properties of the magnetorheological fluid, and that this coefficient influences the rheological shear-resistant properties of the magnetorheological fluid.

In Table 3, a rigorous statistical comparison was performed between the predicted values from the two constitutive models in Figure 7 and the experimental dataset of MRF-132DG magnetorheological fluid. Quantitative evaluations of both the classical single-chain model and the distance-weighted modified model against empirical measurements yielded the following metrics:

Table 3. Comparison of model prediction precision.

Model Type	R-Square	RMSE (kPa)	Explained Value
Single-Chain	−0.9236	27.4017	--(defective)
Distance-Weighted	0.8457	7.7598	84.57%

The computational results in Table 3 demonstrate that the new modified model incorporating interparticle distance weighting accounts for 84.57% σ_y across the experimentally tested strain rate range (γ = 100−800 s^{-1}). It is noteworthy that when predicting the shear stress of MRF-LD132 (39.57 vol.%) using the conventional single-chain model, a negative R^2 value emerged. This provides statistical evidence indicating that the single-chain model may be unable to explicitly explain the physical nature of high-volume-fraction magnetorheological fluids, which is consistent with the conclusions in reference [37,50,51].

5. Conclusions

The inherent limitations of classical single-chain models in predicting shear stress for high-concentration magnetorheological fluids (MRFs) stem from oversimplified treatment of dipole interactions and structural evolution dynamics. Through Monte Carlo simulations augmented with energy barrier analysis, this study fundamentally resolves these deficiencies by establishing a multi-physics-coupled framework that captures three critical phenomena: (1) anisotropic field overlap induced by chain aggregation, (2) non-uniform spatial distribution of magnetization intensity and (3) local dipole rearrangement during structural transitions. The resultant distance-weighted model reduces RMSE by 71.7% compared to conventional approaches, effectively bridging the theoretical-experimental divergence in 30–40 vol.% MRFs.

Central to this advancement is the dual parameterization strategy. The distance-weighting coefficient derived from particle configuration statistics corrects the linear decay assumption of polarization forces. Second, the increment of transverse magnetization explains the phenomenon of the rapid increase in macroscopic shear stress caused by the transition of the chain structure into a network. This is particularly noticeable in the pre-saturation stage, as traditional models incur prediction errors of underprediction exceeding 20% during this stage. Through systematic verification against the data of MRF-132DG material from Lord Corporation, it is found that as the intensity of the external magnetic field increases, the predicted values of the shear stress are in accordance with the variation pattern of the experimental data (R^2 = 0.8457). This finding cannot be explained by the traditional single-chain model (which shows negative R^2 values).

These methodological innovations carry substantial implications for MRF engineering. The validated nonlinear correlation between coating thickness (10–20% range) and shear stress reduction (27.0 ± 2.1%) establishes a predictive framework for tailoring mechanical responses through particle surface modifications. Furthermore, the model's parametric adaptability allows systematic adjustment of distance-weighted interactions and transverse field coupling thresholds. This capability empowers precise tuning of MRF systems operating near critical particle concentrations (30–40 vol.%) where shear stress transitions from chain-controlled to network-governed regimes.

Future expansion research should focus on the influence law of the reconstruction of particles under the action of a magnetic field on the macroscopic mechanical properties under cyclic shear loading. When the magnetic induction intensity B ≥ 0.8 T, the differences between the simulation prediction results (Figure 7) and the experimental data indicate that the problem of prediction errors still partially exists. Incorporating the viscoelastic interactions of the stabilizer layer during the magnetostriction process may further improve the prediction accuracy for industrial-grade magnetorheological fluids (MRFs) operating near the mechanical saturation threshold.

Author Contributions

Conceptualization: L.M. and C.S.; Methodology: L.M. and Y.T.; Software: L.M. and Y.T. and C.C.; Validation: L.M. and Y.T. and Y.H.; Formal Analysis: L.M. and Y.T.; Writing—Original Draft Preparation: Y.T. and L.M.; Writing—Review & Editing: C.S. and L.M.; Visualization: L.M. and P.X.; Supervision: L.M.; Funding Acquisition: Y.H. and P.X.

Ethics Statement

Not applicable.

Informed Consent Statement

Informed consent was obtained from all subjects involved in the study.

Data Availability Statement

No data was used for the research described in the article.

Funding

This research was supported by Xinjiang Uygur Autonomous Region Key Research and Development Project (Grant No.2022B01036).

Declaration of Competing Interest

The authors declare that they have no known competing financial interests or personal relationships that could have appeared to influence the work reported in this paper.

References

1. Long Y, Fei C, Haopeng L. Establishement of Shear Yield Stress Model of Magnetorheological Fluid. *Mater. Mech. Eng.* **2024**, *48*, 86–91. doi:10.11973/jxgccl240117.
2. Liang Z, Yongbao F, Shuzhi L, Zhenxin H, Xiaoxia H. Design of Dynamic Inverse Active Disturbance Rejection Controller for Semi-active MR Suspension System of Heavy Vehicles. *J. Vib. Shock.* **2024**, *43*, 117–125. doi:10.13465/j.cnki.jvs.2024.15.014.

3. Li X, Li P, Dong X. Nonlinear passive magnetorheological damping characteristics of the scissor-like isolation platform. *Arch. Appl. Mech.* **2024**, *94*, 1967–1994. doi:10.1007/s00419-024-02624-3.
4. Chenglong W, Lujie W, Xueqian W, Qingliang Z. New Magneto-inducible Magnetorheological Damper. *J. Vib. Shock.* **2024**, *43*, 248–259. doi:10.13465/j.cnki.jvs.2024.10.029.
5. Wenge S. Designn and Analysis of Magnetorheological. *Clean Coal Technol.* **2024**, *30*, 6–11. doi:10.13226/j.issn.1006-6772.24081503.
6. Goldasz J, Sapinski B. Nondimensional characterization of flow-mode magnetorheological/electrorheological fluid dampers. *J. Intell. Mater. Syst. Struct.* **2012**, *23*, 1545–1562. doi:10.1177/1045389X12447293.
7. Guanghui H, Min W. Study on the Performance of Multi-circular Magnetorheological Fluid Transmission. *Mach. Tool Hydraul.* **2024**, *52*, 162–167.
8. Zuzhi T, Xiangfan W, Fangwei X, Jinjie J, Yangyang G. Time Response Characteristics of Magnetorheological Fluid Transmission Device. *Chin. Hydraul. Pneum.* **2022**, *46*, 190–195. doi:10.11832/j.issn.1000-4858.2022.05.023.
9. Yongliang Z, Keyi W, Shuaishuai Z. Research on Milling of Weak Stiffness Parts Based on Magnetorheological Fluid Auxiliary Support. *J. Mech. Strength* **2022**, *44*, 1057–1063. doi:10.16579/j.issn.1001.9669.2022.05.06.
10. Hesselbach J, Abel-Keilhack C. Active hydrostatic bearing with magnetorheological fluid. *J. Appl. Phys.* **2003**, *93*, 8441–8443. doi:10.1063/1.1555850.
11. Gebreyesus EA, Park A, Guldberg RE, Ong KG. In vitro magnetohydrodynamics system for modulating cell migration. *Biomed. Phys. Eng. Express* **2023**, *9*, 025007. doi:10.1088/2057-1976/acb711.
12. Shahidian A, Ghassemi M, Khorasanizade S, Abdollahzade M, Ahmadi G. Flow Analysis of Non-Newtonian Blood in a Magnetohydrodynamic Pump. *IEEE Trans. Magn.* **2009**, *45*, 2667–2670. doi:10.1109/TMAG.2009.2018954.
13. Sheng R, Flores GA, Liu J. In vitro investigation of a novel cancer therapeutic method using embolizing properties of magnetorheological fluids. *J. Magn. Magn. Mater.* **1999**, *194*, 167–175. doi:10.1016/S0304-8853(98)00565-4.
14. Flores GA, Sheng R, Liu J. Medical applications of magnetorheological fluids a possible new cancer therapy. *J. Intell. Mater. Syst. Struct.* **1999**, *10*, 708–713. doi:10.1106/DJX7-R39A-XKOB-2XAN.
15. Xie M, An Z, Zhuang J. Design and experimental research of dynamic magnetic field device based on Halbach array in magnetorheological polishing. *Int. J. Adv. Manuf. Technol.* **2022**, *120*, 5807–5822. doi:10.1007/s00170-022-09134-y.
16. Zhai Q, Zhai W, Gao B. Investigation on the relationship between apparent viscosity of Fe3O4@SiO2 abrasive-based magneto-rheological fluid and material removal rate of sapphire in magneto-rheological polishing. *Colloids Surf. A: Physicochem. Eng. Asp.* **2022**, *640*, 128420. doi:10.1016/j.colsurfa.2022.128420.
17. Iglesias GR, López-López MT, Durán JDG, González-Caballero F, Delgado AV. Dynamic characterization of extremely bidisperse magnetorheological fluids. *J. Colloid Interface Sci.* **2012**, *377*, 153–159. doi:10.1016/j.jcis.2012.03.077.
18. Shorey AB, Jacobs SD, Kordonski WI, Gans RF. Experiments and observations regarding the mechanisms of glass removal in magnetorheological finishing. *Appl. Opt.* **2001**, *40*, 20–33. doi:10.1364/AO.40.000020.
19. Shaohui Y, Zhiqiang X, Fengjun C, Jianwu Y. Inclined Axis Magnetorheological Finishing Technology for SmallAspherical Surface. *J. Mech. Eng.* **2013**, *49*, 33–38. doi:10.3901/JME.2013.17.033.
20. Barman A, Das M. Design and fabrication of a novel polishing tool for finishing freeform surfaces in magnetic field assisted finishing (MFAF) process. *Precis. Eng.* **2017**, *49*, 61–68. doi:10.1016/j.precisioneng.2017.01.010.
21. Sidpara A, Jain VK. Analysis of forces on the freeform surface in magnetorheological fluid based finishing process. *Int. J. Mach. Tools Manuf.* **2013**, *69*, 1–10. doi:10.1016/j.ijmachtools.2013.02.004.
22. Shen J, Liu S, Yi K, He H, Shao J, Fan Z. Subsurface damage in optical substrates.*Opt. —Int. J. Light Electron Opt.* **2005**, *116*, 288–294. doi:10.1016/j.ijleo.2005.02.002.
23. Zhijun L, Shengyi L, Zhuo W, Xiaoqiang P. Research on the Subsurface Damage during Finishing for Optics. *Aviat. Precis. Manuf. Technol.* **2008**, *44*, 4. doi:10.3969/j.issn.1003-5451.2008.05.001.
24. Shengyi L, Xiaoqiang P. Basic Theory and Method of Controllable Compliant Tools for Optic Elements Manufacturing. *J. Mech. Eng.* **2013**, *49*, 1–9. doi:10.3901/JME.2013.17.001.
25. Yifan D, Xiaoqiang P. Overview of Key Technologies for Optical Manufacturing of Lithographic Projection Lens. *J. Mech. Eng.* **2013**, *49*, 10–18. doi:10.3901/JME.2013.17.010.
26. Saraswathamma K, Jha S, Rao PV. Experimental investigation into Ball end Magnetorheological Finishing of silicon. *Precis. Eng.* **2015**, *42*, 218–223. doi:10.1016/j.precisioneng.2015.05.003.
27. Shiou FJ, Asmare A. Parameters optimization on surface roughness improvement of Zerodur optical glass using an innovative rotary abrasive fluid multi-jet polishing process. *Precis. Eng.* **2015**, *42*, 93–100. doi:10.1016/j.precisioneng.2015.04.004.
28. Rosensweig RE. Basic Equations for Magnetic Fluids with Internal Rotations. *Lect. Notes Phys.* **2002**. doi:10.1007/3-540-45646-5_4.
29. Keaveny EE, Maxey MR. Modeling the magnetic interactions between paramagnetic beads in magnetorheological fluids. *J. Comput. Phys.* **2008**, *227*, 9554–9571. doi:10.1016/j.jcp.2008.07.008.
30. Han Y, Hong W, Faidley LAE. Field-stiffening effect of magneto-rheological elastomers. *Int. J. Solids Struct.* **2013**, *50*, 2281–2288. doi:10.1016/j.ijsolstr.2013.03.030.

31. Jang K-I, Min B-K, Seok J. A behavior model of a magnetorheological fluid in direct shear mode. *J. Magn. Magn. Mater.* **2011**, *323*, 1324–1329. doi:10.1016/j.jmmm.2010.11.039.
32. Ginder JM, Davis LC. Shear stresses in magnetorheological fluids: Role of magnetic saturation. *Appl. Phys. Lett.* **1994**, *65*, 3410–3412. doi:10.1063/1.112408.
33. Hu S, Xianghe P. Roheogical Effect for Magneteroheological Fluids. *J. Chongqing Univ.* **2003**, *26*, 72–75. doi:10.3969/j.issn.1000-582X.2003.05.018.
34. Tang X, Zhang X, Tao R, Rong Y. Structure-enhanced yield stress of magnetorheological fluids. *J. Appl. Phys.* **2000**, *87*, 2634–2638. doi:10.1063/1.372229.
35. Xuli Z, Huimin S, Nannan L, Jie W. Effect of Magnetorheological Fluids with Different Volume Fractions on Shear Properties. *Sci. Technol. Eng.* **2019**, *19*, 183–186.
36. Sarkar C, Hirani H. Effect of Particle Size on Shear Stress of Magnetorheological Fluids. *Smart Sci.* **2015**, *3*, 65–73. doi:10.1080/23080477.2015.11665638.
37. Yingshun Z, Xinlong G, Hui L, Peiqiang Z. Numerical Analysis on Shear Yield Stress of Magnetorheological Fluids. *J. China Univ. Min. Technol.* **2006**, *35*, 498–503. doi:10.3321/j.issn:1000-1964.2006.04.015.
38. Yongzhi L, Xinhua L, Hao L. The Monte Carlo simulation to magnetic particles of magnetorheological fluids. *Procedia Eng.* **2011**, *15*, 3896–3900. doi:10.1016/j.proeng.2011.08.729.
39. Menear S, Bradbury A, Chantrell RW. A model of the properties of colloidal dispersions of weakly interacting fine ferromagnetic particles. *J. Magn. Magn. Mater.* **1984**, *43*, 166–176. doi:10.1016/0304-8853(84)90095-7.
40. Zhuoshan S, Jisheng P, Qiusheng Y. A Review of Research on the Factors Influencing the Stability of Magnetorheological Fluids. *J. Funct. Mater.* **2023**, *54*, 4073–4086. doi:10.3969/j.issn.1001-9731.2023.04.010.
41. Kruse T, Krauthäuser H-G, Spanoudaki A, Pelster R. Agglomeration and chain formation in ferrofluids: Two-dimensional x-ray scattering. *Phys. Rev. B* **2003**, *67*, 094206. doi:10.1103/PhysRevB.67.094206.
42. Donselaar LN, Frederik PM, Bomans P, Buining PA, Humbel BM, Philipse AP. Visualisation of particle association in magnetic fluids in zero-field. *J. Magn. Magn. Mater.* **1999**, *201*, 58–61. doi:10.1016/S0304-8853(99)00118-3.
43. Ginder JM. Behavior of Magnetorheological Fluids. *MRS Bull.* **1998**, *23*, 26–29. doi:10.1557/S0883769400030785.
44. Hui D, Yingshun Z, Xinglong G, Peiqiang Z. Revised Model of the Magnetorhelogical Elastomer Based on Distributed Chains. *Chin. J. Chem. Phys.* **2005**, *18*, 971–975. doi:10.3969/j.issn.1674-0068.2005.06.025.
45. Ivaneyko D, Toshchevikov V, Saphiannikova M, Heinrich G. Effects of particle distribution on mechanical properties of magneto-sensitive elastomers in a homogeneous magnetic field. *Condens. Matter Phys.* **2012**, *15*, 112–116. doi:10.5488/CMP.15.33601.
46. Haitao L, Xianghe P, Weimin C. Yield Shear-stress Model of Magnetorheological Fluids. *Chin. J. Chem. Phys.* **2005**, *18*, 505–509. doi:10.3969/j.issn.1674-0068.2005.04.008.
47. Ma L, Song W, Wang R, Xiu S. Study on shear stress model of magnetorheological fluids with distance weighted factors. *Smart Mater. Struct.* **2017**, *26*, 065009. doi:10.1088/1361-665X/aa6b5e.
48. Haitao L, Xianghe P, Shanglian H. Study on the Chain-formation Mechanism of Magnetorheological Fluids Based on Dipole Theory. *J. Funct. Mater.* **2008**, *39*, 902–904. doi:10.3321/j.issn:1001-9731.2008.06.008.
49. Corp L. *Technical Data: MRF-132DG Magneto-Rheological Fluid*; pp 1–2. Available online: https://www.shoplordmr.com/mr-products/mrf-132dg-magneto-rheological-fluid-250ml (accessed on 15 December 2024).
50. López-López MT, Kuzhir P, Caballero-Hernández J, Rodríguez-Arco L, Duran JDG, Bossis G. Yield stress in magnetorheological suspensions near the limit of maximum-packing fraction. *J. Rheol.* **2012**, *56*. doi:10.1122/1.4731659.
51. Rodríguez-López J, Castro P, Elvira L, Montero de Espinosa F. Study of the effect of particle volume fraction on the microstructure of magnetorheological fluids using ultrasound: Transition between the strong-link to the weak-link regimes. *Ultrasonics* **2015**, *61*, 10–14. doi:10.1016/j.ultras.2015.03.011.